Volume 6
Number 4
21 February 2025
Pages 1203–1542

Materials Advances

rsc.li/materials-advances

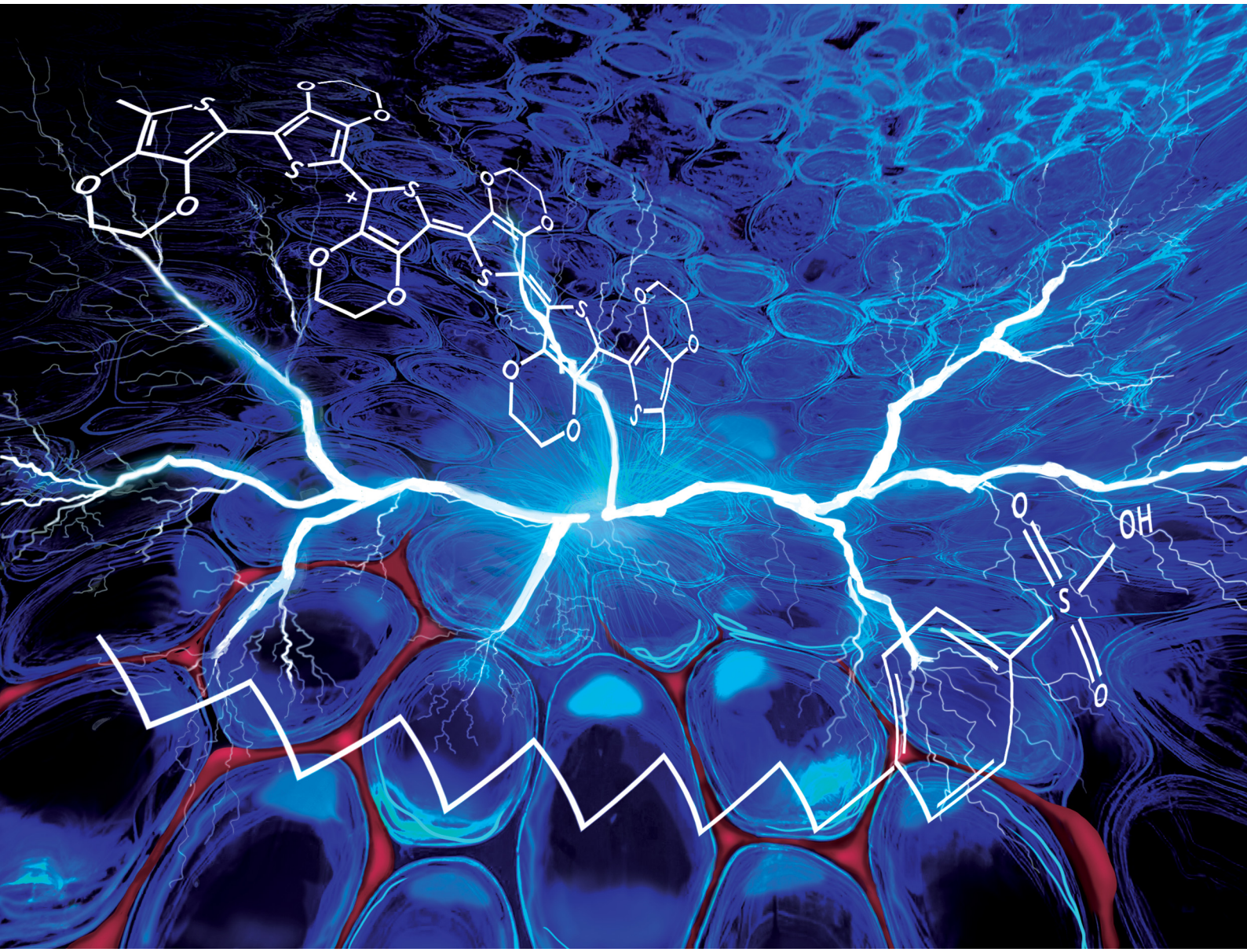

ISSN 2633-5409

ROYAL SOCIETY OF CHEMISTRY

PAPER
Romana Malečková *et al.*
Novel conductive PEDOT:DBSA hydrogels with tuneable properties for bioelectronics

Materials Advances

ROYAL SOCIETY OF CHEMISTRY

PAPER

View Article Online
View Journal | View Issue

Cite this: *Mater. Adv.*, 2025, **6**, 1278

Novel conductive PEDOT:DBSA hydrogels with tuneable properties for bioelectronics†

Romana Malečková, *[a] Šárka Tumová, [a] Petr Smísitel, [b] Jiří Smilek, [a] Helena Šimůnková, [bc] Michaela Pešková, [de] Lubomír Kubáč, [f] Jaromír Hubálek, [bc] Jan Víteček, [d] Martin Vala [a] and Martin Weiter [a]

Conductive hydrogels represent a promising class of novel materials to interface the human body with electronics; however, there is still a high demand for hydrogels that would truly meet the conductivity requirements for efficient signal transmission between the tissues and the device. To address this demand, herein we report the preparation of a novel pure conductive hydrogel based on PEDOT:DBSA at room temperature; thus, we offer an efficient alternative to the commonly used PEDOT:PSS, whose biocompatibility was proven to be limited. With thorough characterization, this work also contributes towards a better understanding of the relationship between the hydrogel structure and electrical properties. The mechanical strength of the novel hydrogel network is tuneable and can be easily tailored to the needs of a given application. Together with an exceptionally low value of Young's modulus, this material provides mechanical properties matching those of soft tissues. Biocompatibility tests confirmed excellent compatibility with murine endothelial cells. The total conductivity of the hydrogel is sufficient for cell-targeted bioelectronic applications, such as cell stimulation; moreover, low impedance was determined at 1 Hz, suggesting that the PEDOT:DBSA hydrogel might offer a truly functional interface between a biological tissue and an electronic device.

Received 30th September 2024,
Accepted 8th January 2025

DOI: 10.1039/d4ma00987h

rsc.li/materials-advances

Introduction

Organic conducting materials have emerged as an alternative to commonly used inorganic materials in a broad range of practical applications (*e.g.* low-cost photovoltaics, flexible touch displays, and OLEDs).[1,2] Moreover, due to their unique properties, these materials stand out especially in the field of bioelectronics. In contrast to rigid inorganic conducting materials, the mechanical properties of organic semiconductors (OSCs) can be tailored to form soft and stretchable films, making them perfect material candidates for applications such as wearable medical devices.[3] Together with the unique ability of some of these materials to conduct both ions and electrons, these materials show the potential to form an interface truly matching those of cells and biological tissue.[4]

Over the last few decades, thin films of OSCs have been used as active layers responsible for communication between tissue and the bioelectronic device. However, the mechanical and physical properties of thin films significantly differ from those of biological tissue, which causes issues at the device–tissue interface, such as inflammatory responses and scar tissue formation, that could lead to deficient signal transmission and reduced device efficacy.[5–7] While biological tissues are generally considered soft, dynamic environments rich in water with a rather low Young's modulus (0.1 kPa to 1 MPa),[8,9] thin films are dry and relatively rigid structures exhibiting a few orders of magnitude higher Young's modulus (from MPa to GPa).[9–12]

In contrast, the hydrogels show mechanical and structural properties similar to those of biological tissues, which perfectly match the environment of living cells.[13,14] Recently, material engineering strategies have been applied to prepare hydrogels with both tissue-like properties and mixed ionic–electronic conductivity of organic semiconductors. Most of these strategies utilized commonly used nature-derived or synthetic non-conductive hydrogels (*e.g.* gelatine or alginate), as the hydrogel matrices interpenetrated with the conducting polymers.[15–18]

[a] *Faculty of Chemistry, Brno University of Technology, Purkyňova 464/118, 612 00 Brno, Czech Republic. E-mail: Romana.Maleckova@vut.cz*
[b] *Central European Institute of Technology, Brno University of Technology, Purkyňova 656/123, 612 00 Brno, Czech Republic*
[c] *Department of Microelectronics, Faculty of Electrical Engineering and Communication, Brno University of Technology, Technická 3058/10, 616 00 Brno, Czech Republic*
[d] *Department of Biophysics of Immune System, Institute of Biophysics of the Czech Academy of Sciences, Královopolská 135, 612 65 Brno, Czech Republic*
[e] *Department of Biochemistry, Faculty of Science, Masaryk University, Kamenice 5, 625 00 Brno, Czech Republic*
[f] *Centre for Organic Chemistry, Rybitví 296, 533 54 Rybitví, Czech Republic*

† Electronic supplementary information (ESI) available. See DOI: https://doi.org/10.1039/d4ma00987h

However, these structures suffer the trade-off between electrical and mechanical properties as they usually contain only units of percent of the conductive material, whose electrical properties are hindered by the insulating matrix.[19] Such hydrogels thus generally show low conductivity. Moreover, doping the hydrogels with a higher amount of conductive polymer negatively affects the mechanical properties of the hydrogel matrix.[19] The discovery of hydrogels purely based on OSCs with tissue-like properties and mixed ionic–electronic conductivity made a breakthrough by allowing the fabrication of highly efficient, easily processed, and tuneable bioelectronic devices and soft robotics, recently reviewed in the literature.[20,21] Thus, these revolutionary hydrogel structures became the main point of interest in the field of bioelectronics, attracting the attention of many scientific groups that introduced various preparation procedures. Yao *et al.* fabricated a hydrogel with electrical conductivity reaching 880 S m^{-1} by mixing PEDOT:PSS with 0.1 M sulfuric acid at elevated temperature (90 °C) with subsequent concentrated sulfuric acid treatment.[22] Lu *et al.* reported a hydrogel prepared by mixing PEDOT:PSS with a volatile DMSO. Subsequent controlled dry annealing at 130 °C and rehydration led to the formation of a hydrogel that exhibited a conductivity of 4×10^3 S m^{-1}.[14] Goestenkors *et al.* studied the properties of PEDOT:PSS hydrogels crosslinked with an ionic liquid, formed after heating the mixture at 60 °C for 15.5 hours, which exhibited excellent cytocompatibility and moderate conductivity up to 127 S m^{-1}.[23] However, all of these techniques required relatively high temperatures, which do not allow the formation of hydrogels in the presence of living cells. Wang *et al.* prepared an ultra-high conductivity pure hydrogel by doping PEDOT:PSS with metal halides, reaching 54.7×10^3 S m^{-1}. However, the hydrogel possesses increased elasticity modulus (10–20 MPa) and inadequate biocompatibility.[24] Moreover, Zhang *et al.*[25] made a remarkable finding when they showed a method of spontaneous gelation of injectable hydrogels at room temperature simply by mixing the PEDOT:PSS suspension with 4-dodecylbenzenesulfonic acid (DBSA) without any other treatment. All of the above-mentioned hydrogels are based on PEDOT:PSS. Although this material is considered to be a gold standard in the field of organic bioelectronics, it was proven that the biocompatibility of this material in the form of a thin film is only limited. This biocompatibility issue is attributed to the presence of the acidic PSS moiety that prevents proper cell adhesion and therefore natural contact of living cells with the material.[15,26,27] This problem limits the potential use of PEDOT:PSS in bioelectronic applications.

Since pure conductive hydrogels are new structures, a deeper understanding is necessary prior to their implementation into bioelectronic systems. However, there are still some challenges that have to be solved to reliably study their properties and potential in bioelectronic applications. One of these challenges is instability that is caused by water evaporation from the hydrogels exposed to air. This causes a gradual change in the hydrogel structure and its properties, which makes measurement of its electrical properties especially very challenging. This is usually solved by using various electrolytes as a medium, using high humidity chambers to prevent air exposure, or simply by characterizing the hydrogels in the dehydrated state.[14,25,28] However, the electrical properties of the swollen hydrogels were shown to be different from those of dried materials (xerogels). Lu *et al.* reported that the electrical conductivity of the pure PEDOT:PSS xerogel was about 5×10^4 S m^{-1}, while the conductivity of the swollen hydrogel dropped significantly, to less than 5×10^3 S m^{-1}.[14] In addition, high humidity can cause corrosion of the measuring equipment in the chamber and the use of excessive aqueous media could cause disruption of the hydrogel network.

Herein, we address the recent challenges of pure conductive hydrogels and present the preparation of a novel, pure PEDOT:DBSA hydrogel. DBSA has already been used as an additive of organic semiconductors showing positive effect on thin film formation, promotion of the film conductivity,[29,30] and as a counterion for polypyrrole, showing excellent biocompatibility of the resulting material.[31,32] In our previous study, we showed that PEDOT:DBSA thin films exhibit improved properties compared to PEDOT:PSS. This novel material stands out mainly thanks to its significantly improved biocompatibility and long-term stability under aqueous conditions. For hydrogel formation, we utilized a previously published technique as we added another DBSA into our PEDOT:DBSA solution, which resulted in a spontaneous sol–gel transition. The addition of DBSA changes the ionic strength in the solution and thus promotes weak interactions between the PEDOT chains, forming a hydrogel network.[25,33] The novel PEDOT:DBSA hydrogel was characterized in detail using PEDOT:PSS as a reference. The detailed analysis of the two hydrogels offers a unique insight into the relationship between the structure and the properties of these interesting structures. In addition, this study provides a knowledge base for the implementation of pure conductive hydrogels in bioelectronic devices. Moreover, in order to address the issue of hydrogel instability, we designed a closed plastic cell, which enables probe measurement under stable experimental conditions.

Experimental section

Materials

PEDOT:DBSA (COC) was synthesised as previously reported.[34] PEDOT:PSS polymer dispersion was purchased from Ossila (M122, PH 1000). DBSA was purchased from Sigma-Aldrich, 44198.

Preparation of the PEDOT:DBSA and PEDOT:PSS hydrogels

The PEDOT:PSS hydrogel was prepared as previously reported,[25] using PEDOT:PSS doped with 3, 5, 8 or 10 v/v% of the secondary dopant, DBSA. The PEDOT:DBSA hydrogel was prepared by doping the suspension of the polymer composite with 3, 5, 8 or 10 v/v% of DBSA (Fig. 1). The mixture of the polymer dispersion and DBSA was agitated until homogenized. After microgel formation, these microgels were separated from excessive media in a centrifuge (Eppendorf MiniSpin®, 12 000 rpm/5 min). The gelation of both hydrogels occurred at room temperature, without the need for any additional treatments. The rheology measurement

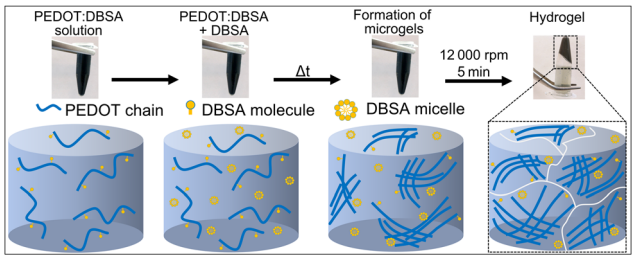

Fig. 1 Proposed formation of the PEDOT:DBSA hydrogel. The addition of DBSA promotes hydrophobic interactions between the PEDOT chains, resulting in the formation of microgels, which are not connected in the whole sample volume.

revealed that the minimal concentration of DBSA added, which led to the induction of the sol–gel transition in the PEDOT:DBSA solution, is 5 v/v%, see Fig. S1, ESI.† Therefore, this concentration was used in the rest of the study. Hydrogels doped with 5 v/v% of the secondary dopant dehydrate at room temperature after 7 and 9 days for PEDOT:DBSA and PEDOT:PSS, respectively.

Biocompatibility testing

To maintain the transparency of the samples, we studied the biocompatibility of both materials in the form of thin films of rehydrated hydrogels. The PEDOT:DBSA xerogel reabsorbed approximately 3% of its original weight during 72 hours after placing the xerogel in the high humidity chamber (humidity >95%). Polymer dispersions and secondary dopant mixtures (5 v/v%) were prepared as described above. The glass cover slides were pretreated by sonication in NaOH and IPA bath for 10 minutes; then, they were rinsed in distilled water and in IPA, and finally air-dried. The mixtures of PEDOT:DBSA and the secondary dopant in liquid form were spin-coated (Laurell, WS-650MZ-8NPPB, 1800 rpm/45 s) on the prepared glass slides after the formation of the microgels. The mixture of PEDOT:PSS and the secondary dopant was spin-coated on the glass slides immediately after these two components were mixed, while the mixture remained liquid. Gelation occurred after spin-coating. Both materials were annealed on a hot plate (Harry Gestigkeit PZ 72, 140 °C, 1 hour) to stabilize them on the glass substrate. This treatment led to the formation of xerogels that were immersed in PBS (1 hour) to remove both the excessive secondary dopant and the excessive PSS molecules. After this, the samples were shortly immersed in IPA to avoid any possible contamination and air-dried.

Mouse pancreatic endothelial cells (MS1, ATCC #CRL-2279) were maintained in high-glucose Dulbecco's modified Eagle medium supplemented with 10% fetal bovine serum, 1% L-glutamine, 1% sodium pyruvate and 1% penicillin–streptomycin (further referred to as the cell culture medium; all components from Gibco-Invitrogen). The xerogels were fixed in a 24-well plate using 1% agarose (VWR, cat. no. 438795A) and rehydrated in the cell culture medium. Cells were plated in a 24-well plate onto rehydrated hydrogels (80 000 cells per well). After 48 hours, the following assays were performed: (i) fluorescein diacetate/propidium iodide (FDA and PI) staining; (ii) 3-(4,5-dimethylthiazol-2-yl)-2,5-diphenyl-2*H*-tetrazolium bromide (MTT) reduction; and (iii) lactate dehydrogenase (LDH) release.

Cell culture medium was replaced with a staining solution (200 µL per well) containing FDA (Sigma-Aldrich, cat. no. F-7378) and PI (Sigma-Aldrich, cat. no. 81845) at final concentrations FDA 0.002 mg mL^{-1} and PI 0.02 mg mL^{-1}, respectively. The staining was carried out in the dark for 5 minutes. After incubation, the staining solution was removed and the cells were washed and observed in PBS (400 µL per well) using a fluorescence microscope (AxioObserver Z1, Carl Zeiss AG, Germany). The culture medium was replaced with a fresh one to which MTT solution (Sigma-Aldrich, cat. no. 13,503-8) was added at a final concentration of 0.125 mg mL^{-1}. After incubation at 37 °C in a 5% CO_2 atmosphere, for 4 hours the medium was aspirated and cells were extracted with 300 µL of 10% Triton X-100 (Sigma-Aldrich, cat. NoT8787) in 0.01M HCl per well on a shaker for 15–20 minutes. The extracts were clarified by centrifugation (5000*g*, 5 min, RT) and the absorbance was measured at 570 nm (Sunrise, Tecan, Switzerland). The cytotoxicity assay was carried out using an LDH kit (Roche, cat. no. 04744934001) according to the manufacturer's instructions. All samples were processed in three independent replicates, each including four parallels per experimental variant. The bar graphs show the mean values and standard deviation (SD; error bars). Outliers were excluded using the Grubbs test. ANOVA with Tukey's *post hoc* HSD test was used to compare the data. All analyses were performed with GraphPad software (GraphPad Software, Inc., USA).

Rheological characterization

The measurement was performed on a DHR2 rheometer (TA Instruments) using steel plate-plate geometry (8 mm diameter, sandblasted, measuring gap 300 µm) at a constant temperature of 25 °C. The sample dimensions are strictly given by this geometry (300 µm in height × 8 mm in diameter). The viscoelastic properties of hydrogels were studied using small-amplitude oscillation shear measurements. The strain sweep test was performed at a constant frequency of oscillation (1 Hz) in the strain range of 0.1–10 000% on a logarithmic scale with 6 points per decade. Before each measurement, the conditioning step (3 min at 25 °C) to relax the sample and temper it to temperature was included during the experiment. Experiments were performed in triplicate using fresh samples for each measurement.

The swelling ratio was determined for hydrogels doped with 5 and 8 v/v% of the secondary dopant (DBSA). The hydrogels were dried at 60 °C for 24 hours and swelled in distilled water for 72 hours. The swelling ratio q was calculated as the ratio of the water weight absorbed by the hydrogel during swelling m_S to the weight of the initial hydrogel m_I: $q = (m_S/m_I) \times 100\%$.

Scanning electron microscopy

The PEDOT:DBSA and PEDOT:PSS hydrogels (both doped with 5 v/v% of DBSA) were prepared in a cylindrical vessel, then cryofixated in liquid nitrogen with subsequent lyophilisation

(SP VirTis AdVantage Pro, SP Scientific). The freeze-dried samples were carefully torn and the sections were gold coated in a sputtering device (Polaron SC7640 sputter coater). The SEM analysis was carried out using a scanning electron microscope ZEISS EVO LS 10 in the mode of secondary electrons (SE), accelerating voltage 5 kV, magnifications 100×, 500×, 1000× and 2000×.

Electrical characterization

For electrical characterization, the hydrogel samples were sealed inside a plastic cell with a channel of 2 mm × 2 mm cross-section (see Fig. S3, ESI†). Galvanically gold-plated tungsten needles were used as electrodes and inserted through wax-sealed cell openings into the hydrogel by an MPS150 probe station performed using Metrohm μAUTOLAB III/FRA2 (5 mm distance between the working electrode (approximately 4 mm^2 active area) and the counter electrode, and 0.5 mm between the quasi reference and working gold electrodes) in the frequency range 0.1 Hz–100 kHz, zero direct current bias. The impedance signal amplitude was 100 mV. The pH of the dispersion sol environments was characterized by a Metrohm 914 pH/conductometer, being 1.4 and 1.36 for PEDOT:DBSA and PEDOT:PSS, respectively. The water content in hydrogels doped with 5 v/v% of DBSA was estimated gravimetrically as 89% in the case of PEDOT:DBSA and 94% in PEDOT:PSS. The total conductivity is equal to $d/(R_1 \cdot S)$, where R_1 is the total resistivity, S is the surface of the working electrode (3.9×10^{-6} m^2) and d is the distance between the working electrode and the auxiliary electrode (5×10^{-3} m).

Results and discussion

Biocompatibility

The compatibility of hydrogels with living cells is one of the fundamental conditions for the use of these materials in regenerative medicine and bioelectronics, in general. Thus, the biocompatibility of the PEDOT:DBSA and the PEDOT:PSS hydrogels toward murine endothelial cells (MS1) was investigated. First, the viability of the cell culture was qualitatively assessed by means of live/dead cell staining; see Fig. 2A. Microscopic observation of stained cells indicated very high cell viability in MS1 cell culture grown on the PEDOT:PSS and the PEDOT:DBSA hydrogels compared to the control (glass cover slide). Indeed, the quantitative determination of relative cell culture viability using the MTT assay supported such observation; see Fig. 2B: the data did not show any significant difference between the hydrogels and the control. Furthermore, the LDH assay, which determines cytotoxicity (*i.e.*, the level of damage to the plasma membrane within a cell population) was used in parallel (Fig. 2C). The PEDOT:DBSA hydrogel induced the same level of cytotoxicity as the control. However, with the PEDOT:PSS hydrogel we observed a slight, however, statistically significant, increase in cytotoxicity compared to the control and to the PEDOT:DBSA. Overall, the data indicate a very high level of biocompatibility of both types of hydrogels, which is comparable to that of standard control. However, as PEDOT:DBSA exhibits lower cytotoxicity, it represents a better interface to biological tissues than the PEDOT:PSS hydrogel.

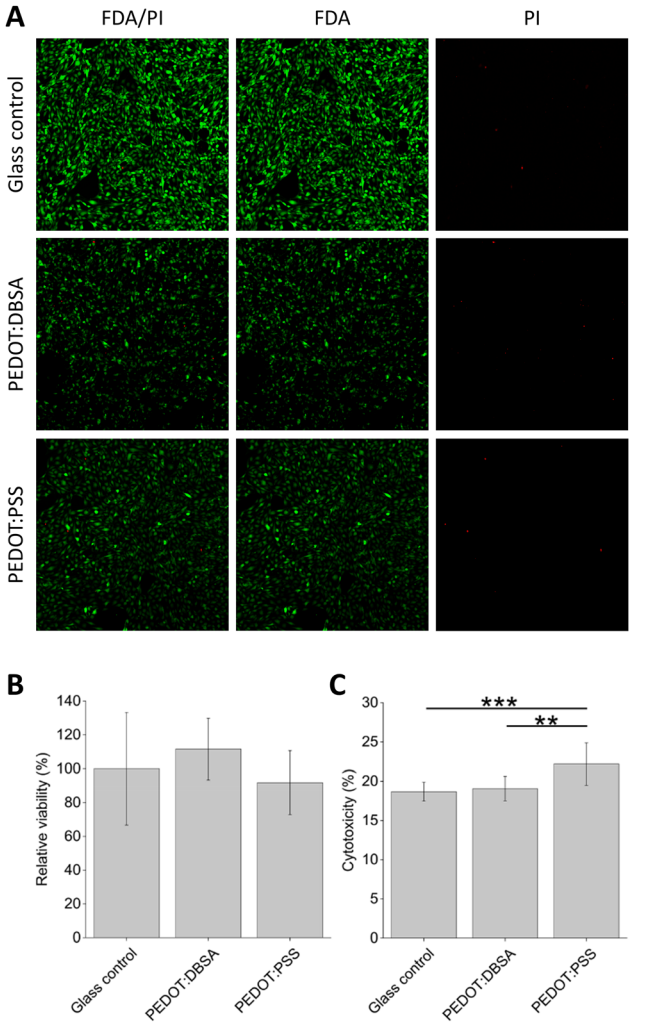

Fig. 2 Biocompatibility assays of the PEDOT:DBSA and the PEDOT:PSS based hydrogels using murine endothelial cells (MS1 line): (A) qualitative assessment of MS1 viability by FDA/PI (live/dead cell) staining. (B) Relative cell culture viability determined by the MTT assay. The viability of the control cell culture represents 100%. (C) Relative cytotoxicity determined by the LDH assay. 100% indicates the maximal extent of cell death on a particular substrate. Data represent mean ± standard deviation (N = 3). Indication of statistically significant difference: $^{**}p < 0.01$, $^{***}p < 0.001$.

Rheological properties

The strain sweep (amplitude) test was used to study the relationship between the mechanical properties and the composition of the prepared hydrogels. The dependences of the storage (G') and loss (G'') modulus on the applied strain (obtained for the individual samples) are depicted in Fig. 3. The minimum concentration of the secondary dopant within the PEDOT:DBSA for gelation to occur was determined as 5 v/v%, see Fig. S1, ESI.† For the PEDOT:PSS, the minimum concentration of the secondary dopant was determined as 3 v/v%, which is in agreement with the literature.[25]

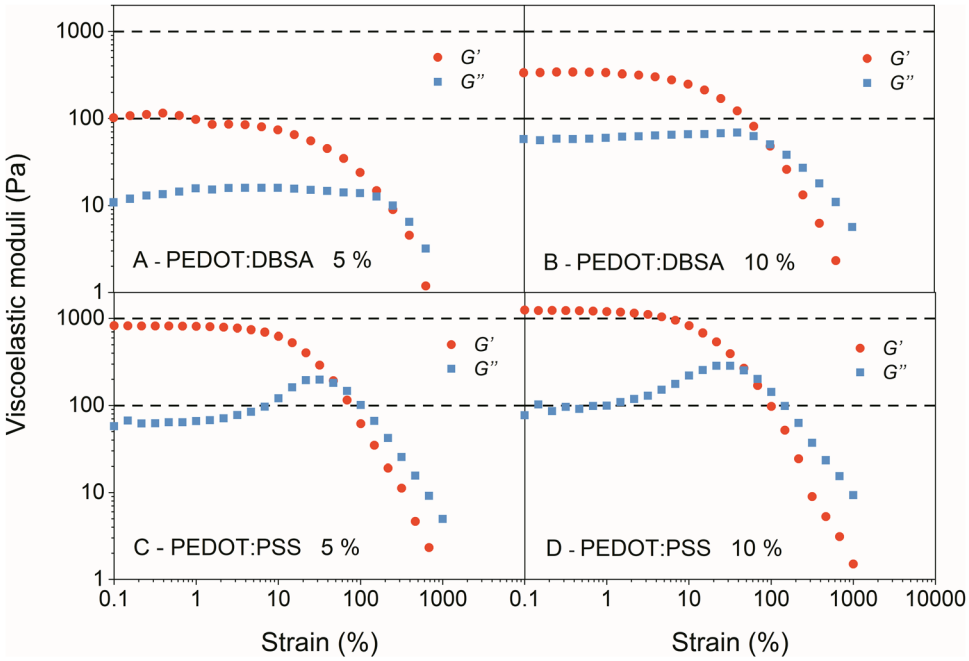

Fig. 3 Strain sweep test of the PEDOT:DBSA and the PEDOT:PSS doped with (A) and (C), 5 v/v% of DBSA; (B) and (D), 10 v/v% of DBSA. G' and G'' show the values of the measured storage and loss modulus, respectively. For better clarity, the dashed line marks the value of viscoelastic moduli of 100 and 1000 Pa.

The lower values of both G' and G'' moduli in the PEDOT:DBSA hydrogels (Fig. 3A) indicate a lower mechanical strength of these structures. The position of the end of the linear viscoelastic region (LVO) (the end of a region, where G' and G'' are linear) indicates the strength of the newly emerging hydrogel bonds. A similar position of the LVO end with respect to the x-axis for both samples (regardless of the DBSA concentration) suggests that both hydrogels are formed by bonds of the same electrostatic nature. With increasing DBSA concentration, a higher value of both G' and G'' moduli was observed (see Fig. 3B and D); a similar trend was detected in both materials.

The observed results indicate a similar mechanism of hydrogel formation for both materials as they contain bonds of the same electrostatic nature. However, in the case of PEDOT:DBSA, this mechanism leads to the formation of microgels that are mechanically pressed together during centrifugation, but there is no physical bond between these microgels. This corresponds to the lower mechanical strength of this type of hydrogel as lower moduli indicate less nodes in hydrogel structure and therefore the lower level of crosslinking density.[35] We hypothesize that these differences in hydrogel crosslinking and thus in their mechanical strength are caused by the structural dissimilarities of PEDOT counterions. While the DBSA counterion is a single molecule, PSS forms long chains that can intertwine and thus increase the total number of physical bonds. This contributes to the formation of the hydrogel network in the whole bulk and to the higher mechanical strength of the resulting 3D network.

Since the increase of added DBSA leads to the improved mechanical strength of hydrogels, it suggests that the higher amount of the secondary dopant further weakens the interaction between PEDOT chains and primary dopant, PSS or DBSA in PEDOT:PSS or PEDOT:DBSA, respectively. As a result, the hydrophobic interactions and π–π stacking between the PEDOT chains are strengthened, and become physically more intertwined, resulting in a denser hydrogel structure that is also mechanically stronger and more rigid. This significant increase in the values of both moduli at higher dopant concentrations (10 v/v%) indicates that only a simple adjustment during the preparatory process can result in the production of a hydrogel with completely different viscoelastic behaviour. Hence, it is possible to use this simple yet effective procedure to tailor the crosslinking degree of the gel network exactly to the needs of the required application. The swelling ratio for hydrogels doped with 5 v/v% of the secondary dopant was determined as $(15.6 \pm 1.4)\%$ and $(20 \pm 2)\%$ for PEDOT:DBSA and PEDOT:PSS, respectively. At a higher secondary dopant content (8 v/v%), the swelling ratio increased slightly in both hydrogels on $(25 \pm 4)\%$ in PEDOT:DBSA and $(28 \pm 4)\%$ in PEDOT:PSS. Usually, the higher degree of crosslinking results in a lower swelling ability.[36] The increase in the swelling ratio in the investigated hydrogels may be caused by an increased amount of free sulfonate groups from dopant molecules, as manipulation of the sulfonate groups in the hydrogel can increase its swelling ability.[37]

Young's modulus

Young's modulus (the ability of a material to resist mechanical stress) is one of the key features of a material that interfaces biological tissues. Young's modulus was determined using

Table 1 Young's modulus measured for the PEDOT:DBSA and the PEDOT:PSS hydrogels (mean ± S.D.) with different secondary dopant content

Material	Dopant content (v/v%)	Young's modulus (kPa)
PEDOT:DBSA	5	1.5 ± 0.2
	10	1.2 ± 0.1
PEDOT:PSS	5	1.49 ± 0.08
	10	1.6 ± 0.1

dynamic mechanical analysis to obtain a result that would correspond to the properties of the bulk material. For the PEDOT:DBSA and PEDOT:PSS hydrogels doped with 5 v/v% of the secondary dopant, it was determined as (1.5 ± 0.2) kPa and (1.49 ± 0.08) kPa, respectively, see Table 1. For the PEDOT:PSS hydrogel, we observed that the higher the amount of the secondary dopant in the material, the higher the Young's modulus and the higher the ability to withstand mechanical stress. Interestingly, we did not observe this tendency with the PEDOT:DBSA hydrogel, where Young's modulus of the hydrogel doped with 10 v/v% of the dopant decreased in comparison with the PEDOT:DBSA doped with 5 v/v% of the dopant. The strain sweep test proved that, at higher dopant concentrations, a denser hydrogel network is formed; it is more resistant to mechanical stress. Thus, we expected higher Young's moduli at higher dopant concentrations. We hypothesise that when PEDOT:DBSA is doped with 10 v/v% of DBSA, most of the polymer chains are saturated and cannot bind more of the dopant. Consequently, if stress occurs, excessive dopant molecules can be pushed to the surface of the gel, where they act as a lubricant and interfere with the measurement.

The values of Young's moduli determined for both hydrogels are within the range given for the most of the soft tissues (0.1–100 kPa),[8,38] and therefore represent a significant improvement of mechanical properties of the investigated materials compared to those of commonly used thin films with Young's modulus in the range of 100 MPa–10 GPa.[39,40] Young's moduli of both hydrogels are similar to Young's modulus of the brain (1.4–3.7 kPa[38]), thus its use could be especially advantageous when stimulating these sensitive areas.

Morphology of the hydrogels

The internal structure of the lyophilized xerogels was analysed by scanning electron microscopy (SEM); it is shown in Fig. 4. The PEDOT:PSS xerogel demonstrates smooth morphology (Fig. 4D–F), resembling connected fibres. Holes and cavities in the range of tens of micrometres are clearly visible at lower magnifications (Fig. 4E and F). The PEDOT:DBSA xerogel (Fig. 4A–C) shows a much rougher structure, which seems to comprise many smaller consistent parts of various sizes separated by cavities, reminding of a sponge, clearly arranged in one direction.

The differences observed in the hydrogels studied support the results of the rheological characterization. The hydrogel structure of PEDOT:PSS consists of a network of connected hydrophobic PEDOT chains, but the whole structure can be supported by physically intervened long PSS chains, forming a more interconnected, mechanically stronger morphology. On the other hand, in the PEDOT:DBSA hydrogel, the additional supporting network molecules are missing because the DBSA molecules are not polymerized. Thus, the morphology is a result of centrifugation of the microgels.

Several studies have already shown that rough morphology on a micron scale was proven to have a positive effect on cell adhesion of many cell types, including endothelial cells.[41–43] Hence, the experiment shows that PEDOT:DBSA possesses a promising morphology (and, as previous analyses showed, also mechanical properties) for cell adhesion and proliferation.

Electrical properties

Impedance spectroscopy (IS) was used to envision processes occurring within prepared hydrogels, as this technique takes into account electron transfer as well as capacitance effects; moreover, the materials can be investigated under biologically relevant low frequencies.[15,44] Therefore, IS was used to characterize electronic and ionic conductivity of the hydrogels and to study their impedance as a function of frequency.

The IS was performed using the PEDOT:DBSA and PEDOT:PSS hydrogels (both with 5 v/v% of secondary dopant) as ''gel/solid'' electrolyte. The hydrogel was sealed inside a measuring cell with electronically conducting electrodes on its two sides, see Fig. S3, ESI.†

The mixed ionic–electronic conductivity of PEDOT-based composites was determined in previous studies.[45] The complex impedance plots of our PEDOT hydrogels remind two semicircles, as shown in Fig. 5A and B. The first real-axis intercept was measuring the cell serial resistance, the second one the total resistance R_1, which equalled to a parallel combination of R_i (ionic) and R_e (electronic) $- R_iR_e/(R_i + R_e)$. The total conductivity equals $d/(R_1 \cdot S)$. Hydrogels doped with 5 v/v% of the secondary dopant exhibited a total conductivity up to 36 S m^{-1} (with an average value of 22 ± 10 S m^{-1}) and 724 S m^{-1} (with an average value of 523 ± 217 S m^{-1}) for PEDOT:DBSA and PEDOT:PSS, respectively see Fig. S5, ESI.† The total conductivity was further determined at an enhanced secondary dopant concentration (8%). Both hydrogels exhibited increased conductivity up to 99 S m^{-1} for PEDOT:DBSA (with an average value of 65 ± 28 S m^{-1}) and 1327 S m^{-1} for PEDOT:PSS (with an average value of 888 ± 411 S m^{-1}).

Since low frequency stimulation is common in regenerative medicine and tissue engineering (~0.1–10 Hz),[46] the impedance of PEDOT:DBSA and PEDOT:PSS at 1 Hz was evaluated, being 0.17 Ω m and 0.01 Ω m, respectively. Both prepared hydrogels showed low impedance at 1 Hz, compared to PEDOT:PSS in a typical interpenetrating network with a non-conductive hydrogel matrix, with impedance at least 2 orders of magnitude higher (measured in a similar experimental setup.[15]

The conductivity measurement revealed a prevailing ionic conductivity (2 times higher than the electronic one) in the PEDOT:DBSA hydrogel. In the PEDOT:PSS hydrogel, electrical conductivity prevailed (6 times as high as the ionic one). The prevailing ionic conductivity in the case of the novel

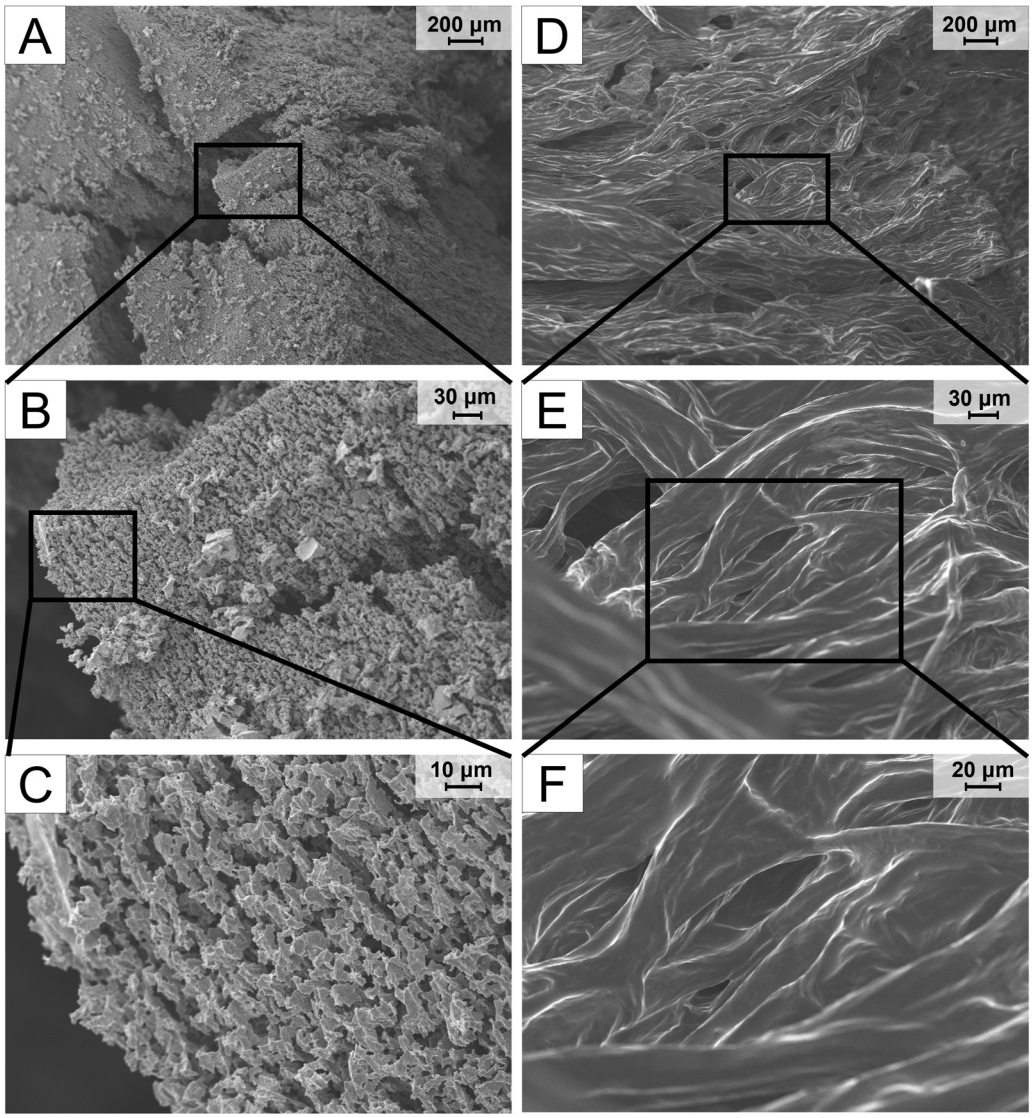

Fig. 4 Cross-section of lyophilized xerogels of PEDOT:DBSA (A)–(C) and of PEDOT:PSS (D)–(F), both doped with 5 v/v% of DBSA. Both samples are shown in three magnifications, so that the wider surroundings (100×; (A) and (D)) can be seen, as well as the details of the structure ((C) 2000×; (F) 1000×).

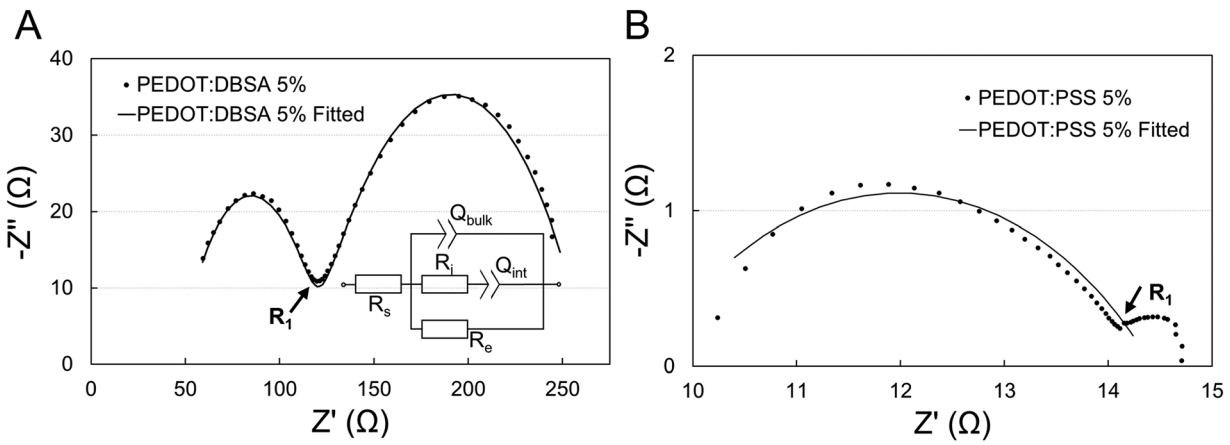

Fig. 5 Complex impedance plots of (A) – the PEDOT:DBSA and (B) – the PEDOT:PSS hydrogel measured and fitted with the inserted equivalent circuit at zero DC bias. R_s stands for serial contact resistance; R_i stands for ionic resistance; and R_e for electronic resistance. The total resistance of the hydrogels was determined as $R_1 = R_iR_e/(R_e + R_i)$.

Table 2 The comparison of selected material properties of pure PEDOT:DBSA hydrogel and recently published pure hydrogels based on PEDOT (2–6) and selected IPN hydrogels based on PEDOT (7–10)

Entry	Components	Young's modulus (kPa)	Conductivity (S cm^{-1})	Biocompatibility	Intended application	Ref.
1[a]	PEDOT:DBSA, DBSA	1.5 ± 0.2	Up to 1	Good with MS1 line	Cell-targeted bioelectronic applications	—
2	PEDOT:PSS, DBSA	~1	~0.1	Good with C2C12 line	Hydrogel-fiber based OECT	25
3	PEDOT:PSS, DMSO	~2×10^3	40	N/A	Bioelectronic devices and applications	14
4	PEDOT:PSS, sulphuric acid	N/A	8.8	N/A	Electrocatalysis, sensors, actuators	22
5	PEDOT:PSS, metal halides	10^4–20^4	Up to 547	Harmful to the tissues	Thermotherapy, flexible electronics	24
6	PEDOT:PSS, ionic liquids	Up to 4.13 ± 1.63	Up to 1.27 ± 0.75	Good with NHDF cells	Biointerfacing of bioelectronic devices	23
7	PEDOT:PSS, GelMA	7.6 ± 2.3–10.3 ± 2.7	N/A	Good with C2C12 line	On-skin electrodes, neural probes	15
8	PAA/PEDOT:PSS	~10	Up to 0.0183	Good with HSF cells	Body-conformable electronics	53
9	PEDOT:PSS, silk fibroin, PVA/PAM	24–128	Up to 0.0521	Good with NIH3T3 cells	Flexible electronics	54
10	PEDOT:PSS, PVA	~460	~10	Low cytotoxicity	Stretchable bioelectronics	55

[a] This work.

PEDOT:DBSA hydrogel might be related to the lower crosslinking density in the hydrogel network compared to that of the PEDOT:PSS, which might allow for smooth movement of ions across the hydrogel structure. The improved total conductivity at higher secondary dopant concentrations (8 v/v%) in both materials is related to the higher crosslinking density in the hydrogel structures, as confirmed by rheological testing and reported for pure hydrogels in the literature.[23] In more crosslinked structures, PEDOT chains are in the closer proximity, leading to the conductivity enhancement.[47] Although the total conductivity of the PEDOT:DBSA hydrogel is lower compared to some of the other pure hydrogels based on PEDOT (see Table 2) it is similar[48] or more than 4 orders of magnitude higher than the conductivity of materials successfully used for cell stimulation[49–51] and is higher than conductivity of the cerebrospinal fluid (1.54 S m^{-1}), which represents the human tissue with the highest conductivity.[52] Therefore, we assume that this novel hydrogel offers an electrical microenvironment suitable for cell stimulation.

Conclusions

In summary, we prepared a conductive hydrogel based on the novel material PEDOT:DBSA, where DBSA serves as both a counterion for PEDOT and an efficient secondary dopant inducing the gelation process without the need for elevated temperatures. We studied its properties in detail together with those of the PEDOT:PSS hydrogel, which served as a reference prepared in the same manner.

It was shown that the different structure of counterions in the studied materials significantly affects the resulting properties of formed hydrogels. The PEDOT:DBSA hydrogel showed better biocompatibility compared to the PEDOT:PSS counterpart since the LDH assay revealed a higher cytotoxic effect of the latter mentioned. The rheological characterization showed that the hydrogel network of the PEDOT:DBSA possesses lower crosslinking density than that of PEDOT:PSS. The above might be due to the fact that in the PEDOT:DBSA, the counterion molecules (DBSA) are not connected in the same way as in the PEDOT:PSS; therefore, they do not provide additional mechanical support to the hydrogel. In both materials, the mechanical strength can be easily tailored by adjusting the amount of the secondary dopant inducing the gelation. This is an important feature especially for the field of bioelectronics regenerative medicine, where finding a material with properties closely matching the viscoelastic behaviour of a given tissue is a key step to forming a matching electronic-tissue interface. The Young's modulus of PEDOT:DBSA and that of PEDOT:PSS hydrogels is in the range of the modulus of soft biological tissues, which indicates a suitable softness of both materials to interface living cells. Impedance spectroscopy disclosed suitable mixed ionic–electronic conductivity of both hydrogels for cell-targeted bioelectronic applications. The total conductivity can be improved by manipulating the concentration of the secondary dopant while maintaining the soft mechanical properties, crucial for interfacing biological tissues. Both hydrogels show a low impedance at a frequency of 1 Hz, which is an important factor in increasing the signal-to-noise ratio between the material and the tissue.

To summarize, a new pure hydrogel based on PEDOT:DBSA was prepared in a facile way; it possesses tunable mechanical and electrical properties and excellent biocompatibility. We believe that the application of this new hydrogel material might give rise to the implementation of more efficient bioelectronic devices with better applicability in cell-targeted bioelectronic applications and stimulation of a wide range of cell types.

Author contributions

R. M.: conceptualization, investigation, formal analysis, methodology, writing – original draft, writing – review & editing, visualization, funding acquisition. Š. T.: conceptualization, investigation, formal analysis, methodology, writing – review & editing, funding acquisition. P. S.: investigation, methodology, funding acquisition. J. S.: investigation, formal analysis, methodology, writing – review & editing. H. Š.: formal analysis, writing – original draft, writing – review & editing. Michaela Pešková: investigation, formal analysis, writing – review & editing.

L. K.: conceptualization, writing – review & editing. J. H.: supervision, writing – review & editing. M. V.: conceptualization, supervision, writing – review & editing. M. W.: conceptualization, supervision, writing – review & editing, funding acquisition.

Data availability

Research data are available from **https://doi.org/10.5281/zenodo.14565833** or from the author. The data supporting this article have been included as part of the ESI.†

Conflicts of interest

There are no conflicts to declare.

Acknowledgements

This work was supported by the Czech Science Foundation grant no. 21-01057S, the rheological characterization (J. Smilek) and ionic conductivity studies was subsequently supported by the Czech Science Foundation grant no. 24-10469S. R. Malečková, Š. Tumová and P. Smísitel also acknowledge the internal support of Brno University of Technology, project CEITEC VUT/FCH-J-21-7268. The authors also acknowledge Ing. Monika Trudičová, PhD, for the SEM analysis and doc. Vojtěch Enev, PhD, for sample lyophilization.

References

1 K. Liu, B. Ouyang, X. Guo, Y. Guo and Y. Liu, *npj Flexible Electron.*, 2022, **6**, DOI: **10.1038/s41528-022-00133-3**.
2 C. Liu, C. Xiao, C. Xie and W. Li, *Nano Energy*, 2021, **89**, 106399, DOI: **10.1016/j.nanoen.2021.106399**.
3 X. Zhou, P. Kateb, J. Fan, J. Kim, G. A. Lodygensky, B. Amilhon, D. Pasini and F. Cicoira, *J. Mater. Chem. C*, 2024, **12**, 5708–5717, DOI: **10.1039/D3TC04230H**.
4 D. T. Simon, E. O. Gabrielsson, K. Tybrandt and M. Berggren, *Chem. Rev.*, 2016, **116**, 13009–13041, DOI: **10.1021/acs.chemrev.6b00146**.
5 Z. Hao, S. Wang, K. Zhang, J. Zhou, D. Li, J. He, L. Gao and L. Wang, *Materials*, 2021, **14**, 4718, DOI: **10.3390/ma14164718**.
6 C. Marin and E. Fernandez, *Front. Neuroeng.*, 2010, **8**, DOI: **10.3389/fneng.2010.00008**.
7 A. Sridharan, S. D. Rajan and J. Muthuswamy, *J. Neural Eng.*, 2013, **10**, 066001, DOI: **10.1088/1741-2560/10/6/066001**.
8 J. Liu, H. Zheng, P. Poh, H. G. Machens and A. Schilling, *Int. J. Mol. Sci.*, 2015, **16**, 15997–16016, DOI: **10.3390/ijms160715997**.
9 R. Feiner and T. Dvir, *Nat. Rev. Mater.*, 2018, **3**, 17076, DOI: **10.1038/natrevmats.2017.76**.
10 J. Rivnay, H. Wang, L. Fenno, K. Deisseroth and G. G. Malliaras, *Sci. Adv.*, 2017, **3**, e1601649, DOI: **10.1126/sciadv.1601649**.
11 P. Kateb, J. Fan, J. Kim, X. Zhou, G. A. Lodygensky and F. Cicoira, *Flexible Printed Electron.*, 2023, **8**, 045006, DOI: **10.1088/2058-8585/ad05d6**.
12 J. Kim, J. Fan, G. Petrossian, X. Zhou, P. Kateb, N. Gagnon-Lafrenais and F. Cicoira, *Mater. Horiz.*, 2024, **11**, 3548–3560, DOI: **10.1039/D4MH00203B**.
13 V. R. Feig, H. Tran, M. Lee and Z. Bao, *Nat. Commun.*, 2018, **9**, 2740, DOI: **10.1038/s41467-018-05222-4**.
14 B. Lu, H. Yuk, S. Lin, N. Jian, K. Qu, J. Xu and X. Zhao, *Nat. Commun.*, 2019, **10**, 1043, DOI: **10.1038/s41467-019-09003-5**.
15 A. R. Spencer, A. Primbetova, A. N. Koppes, R. A. Koppes, H. Fenniri and N. Annabi, *ACS Biomater. Sci. Eng.*, 2018, **4**, 1558–1567, DOI: **10.1021/acsbiomaterials.8b00135**.
16 F. Fu, J. Wang and J. Yu, *J. Mater. Chem. C*, 2021, **9**, 11794–11800, DOI: **10.1039/D1TC01578H**.
17 K. Wang, L. Tian, T. Wang, Z. Zhang, X. Gao, L. Wu, B. Fu and X. Liu, *Compos. Interfaces*, 2018, **26**, 27–40, DOI: **10.1080/09276440.2018.1465766**.
18 J. Duan, X. Liang, J. Guo, K. Zhu and L. Zhang, *Adv. Mater.*, 2016, **28**, 8037–8044, DOI: **10.1002/adma.201602126**.
19 H. Yuk, B. Lu and X. Zhao, *Chem. Soc. Rev.*, 2019, **48**, 1642–1667, DOI: **10.1039/C8CS00595H**.
20 H. Li, J. Cao, R. Wan, V. R. Feig, C. M. Tringides, J. Xu, H. Yuk and B. Lu, *Adv. Mater.*, 2024, 2415151, DOI: **10.1002/adma.202415151**.
21 J. Li, J. Cao, B. Lu and G. Gu, *Nat. Rev. Mater.*, 2023, **8**, 604–622, DOI: **10.1038/s41578-023-00587-5**.
22 B. Yao, H. Wang, Q. Zhou, M. Wu, M. Zhang, C. Li and G. Shi, *Adv. Mater.*, 2017, **29**, 1700974, DOI: **10.1002/adma.201700974**.
23 A. P. Goestenkors, T. Liu, S. S. Okafor, B. A. Semar, R. M. Alvarez, S. K. Montgomery, L. Friedman and A. L. Rutz, *J. Mater. Chem. B*, 2023, **11**, 11357–11371, DOI: **10.1039/D3TB01415K**.
24 H. Wang, T. Zhuang, J. Wang, X. Sun, Y. Wang, K. Li, X. Dai, Q. Guo, X. Li, D. Chong, B. Chen and J. Yan, *Adv. Mater.*, 2023, **35**, 2302919, DOI: **10.1002/adma.202302919**.
25 S. Zhang, Y. Chen, H. Liu, Z. Wang, H. Ling, C. Wang, J. Ni, B. Çelebi-Saltik, X. Wang, X. Meng, H. J. Kim, A. Baidya, S. Ahadian, N. Ashammakhi, M. R. Dokmeci, J. Travas-Sejdic and A. Khademhosseini, *Adv. Mater.*, 2020, **32**, 1904752, DOI: **10.1002/adma.201904752**.
26 D. Mantione, I. del Agua, W. Schaafsma, J. Diez-Garcia, B. Castro, H. Sardon and D. Mecerreyes, *Macromol. Biosci.*, 2016, **16**, 1227–1238, DOI: **10.1002/mabi.201600059**.
27 E. Šafaříková, L. Švihálková Šindlerová, S. Stříteský, L. Kubala, M. Vala, M. Weiter and J. Víteček, *Sens. Actuators, B*, 2018, **260**, 418–425, DOI: **10.1016/j.snb.2017.12.108**.
28 X. Ren, M. Yang, T. Yang, C. Xu, Y. Ye, X. Wu, X. Zheng, B. Wang, Y. Wan and Z. Luo, *ACS Appl. Mater. Interfaces*, 2021, **21**, 25374–25382, DOI: **10.1021/acsami.1c04432**.
29 M. Sessolo, D. Khodagholy, J. Rivnay, F. Maddalena, M. Gleyzes, E. Steidl, B. Buisson and G. G. Malliaras, *Adv. Mater.*, 2013, **25**, 2135–2139, DOI: **10.1002/adma.201204322**.
30 S. Zhang, P. Kumar, A. S. Nouas, L. Fontaine, H. Tang and F. Cicoira, *APL Mater.*, 2015, **3**, 014911, DOI: **10.1063/1.4905154**.

31 A. Fahlgren, C. Bratengeier, A. Gelmi, C. M. Semeins, J. Klein-Nulend, E. W. H. Jager, A. D. Bakker and G. Papaccio, *PLoS One*, 2015, **10**, e0134023, DOI: 10.1371/journal.pone.0134023.
32 B. C. Thompson, S. E. Moulton, R. T. Richardson and G. G. Wallace, *Biomaterials*, 2011, **32**, 3822–3831, DOI: 10.1016/j.biomaterials.2011.01.053.
33 B. Zhao, Z. Li, L. Zheng, Z. Ye, Y. Yuan, S. Zhang, B. Liang and T. Li, *Chin. Chem. Lett.*, 2024, **35**, 109810, DOI: 10.1016/j.cclet.2024.109810.
34 Š. Tumová, R. Malečková, L. Kubáč, J. Akrman, V. Enev, L. Kalina, E. Vojtková, M. Pešková, J. Víteček, M. Vala and M. Weiter, *Polym. J.*, 2023, **55**, 983–995, DOI: 10.1038/s41428-023-00784-7.
35 L. Pescosolido, L. Feruglio, R. Farra, S. Fiorentino, I. Colombo, T. Coviello, P. Matricardi, W. E. Hennink, T. Vermonden and M. Grassi, *Soft Matter*, 2012, **8**, 7708–7715, DOI: 10.1039/c2sm25677k.
36 P. N. Dave and A. Gor, *Handbook of Nanomaterials for Industrial Applications – A volume in Micro and Nano Technologies*, Elsevier, 2018, pp. 36–66, DOI: 10.1016/B978-0-12-813351-4.00003-1.
37 L. Brelle, F. Faÿ, T. Ozturk, N. Didier, E. Renard and V. Langlois, *Biomacromolecules*, 2023, **24**, 1871–1880, DOI: 10.1021/acs.biomac.3c00059.
38 G. Singh and A. Chanda, *Biomed. Mater.*, 2021, **16**, 062004, DOI: 10.1088/1748-605X/ac2b7a.
39 M. ElMahmoudy, V. F. Curto, M. Ferro, A. Hama, G. G. Malliaras, R. P. O'Connor and S. Sanaur, *J. Appl. Polym. Sci.*, 2019, **136**, 47029, DOI: 10.1002/app.47029.
40 U. Lang, N. Naujoks and J. Dual, *Synth. Met.*, 2009, **159**, 473–479, DOI: 10.1016/j.synthmet.2008.11.005.
41 K. Zhou, Y. Li, L. Zhang, L. Jin, F. Yuan, J. Tan, G. Yuan and J. Pei, *Bioact. Mater.*, 2021, **6**, 262–272, DOI: 10.1016/j.bioactmat.2020.08.004.
42 S. Zijl, A. S. Vasilevich, P. Viswanathan, A. L. Helling, N. R. M. Beijer, G. Walko, C. Chiappini, J. de Boer and F. M. Watt, *Acta Biomater.*, 2019, **84**, 133–145, DOI: 10.1016/j.actbio.2018.12.003.
43 C. Simitzi, A. Ranella and E. Stratakis, *Acta Biomater.*, 2017, **51**, 21–52, DOI: 10.1016/j.actbio.2017.01.023.
44 R. D. Breukers, K. J. Gilmore, M. Kita, K. K. Wagner, M. J. Higgins, S. E. Moulton, G. M. Clark, D. L. Officer, R. M. I. Kapsa and G. G. Wallace, *J. Biomed. Mater. Res., Part A*, 2010, **95A**, 256–268, DOI: 10.1002/jbm.a.32822.
45 R. Del Olmo, N. Casado, J. L. Olmedo-Martínez, X. Wang and M. Forsyth, *Polymers*, 2020, **12**, 1981, DOI: 10.3390/polym12091981.
46 L. P. da Silva, S. C. Kundu, R. L. Reis and V. M. Correlo, *Trends Biotechnol.*, 2020, **38**, 24–49, DOI: 10.1016/j.tibtech.2019.07.002.
47 M. Modarresi and I. Zozoulenko, *Phys. Chem. Chem. Phys.*, 2022, **24**, 22073–22082, DOI: 10.1039/D2CP02655D.
48 Y. Han, M. Sun, X. Lu, K. Xu, M. Yu, H. Yang and J. Yin, *Composites, Part B*, 2024, **273**, 111241, DOI: 10.1016/j.compositesb.2024.111241.
49 A. Babaie, B. Bakhshandeh, A. Abedi, J. Mohammadnejad, I. Shabani, A. Ardeshirylajimi, S. R. Moosavi, J. Amini and L. Tayebi, *Eur. Polym. J.*, 2020, **140**, 110051, DOI: 10.1016/j.eurpolymj.2020.110051.
50 C. T. Liu, J. Yu, M. H. Lin, K. H. Chang, C. Y. Lin, N. C. Cheng, P. I. Wu, C. W. Huang, P. Y. Zhang, M. T. Hung and Y. S. Hsiao, *Biomacromolecules*, 2023, **24**, 3858–3871, DOI: 10.1021/acs.biomac.3c00506.
51 Y. C. Chen, Y. F. Lin, C. T. Liu, Y. C. Liu, M. H. Lin, G. Y. Lan, Y. S. Cheng, H. L. Yu, C. C. Huang, H. T. Chang, N. C. Cheng, Y. S. Hsiao and J. Yu, *ACS Appl. Polym. Mater.*, 2023, **5**, 4753–4766, DOI: 10.1021/acsapm.3c00146.
52 C. Ramon, J. Haueisen and P. H. Schimpf, *Biomed. Eng. Online*, 2006, **5**, DOI: 10.1186/1475-925X-5-55.
53 Q. Gao, C. Li, M. Wang, J. Zhu and C. Gao, *J. Mater. Chem. C*, 2023, **11**, 9355–9365, DOI: 10.1039/D3TC00850A.
54 J. Yang, Y. Fan, X. Xiong, Q. Jiang, P. Li, J. Jian and L. Chen, *Appl. Phys. A: Mater. Sci. Process.*, 2024, **130**, 157, DOI: 10.1007/s00339-024-07329-6.
55 G. Li, K. Huang, J. Deng, M. Guo, M. Cai, Y. Zhang and C. F. Guo, *Adv. Mater.*, 2022, **34**, 2200261, DOI: 10.1002/adma.202200261.